Quaternary Science Reviews 259 (2021) 106907

Contents lists available at ScienceDirect

Quaternary Science Reviews

journal homepage: www.elsevier.com/locate/quascirev

Magnetostratigraphy and cosmogenic dating of Wonderwerk Cave: New constraints for the chronology of the South African Earlier Stone Age

Ron Shaar [a, *], Ari Matmon [a], Liora K. Horwitz [b], Yael Ebert [a], Michael Chazan [d], ASTER Team[c]

[a] The Institute of Earth Sciences, The Hebrew University of Jerusalem, Jerusalem, 91904, Israel
[b] National Natural History Collections, The Hebrew University, Jerusalem, 91904, Israel
[c] CEREGE, UMR 6635 CNRS-Aix-Marseille University, BP 80, 13 545 Aix en Provence, Cedex 4, France
[d] Department of Anthropology, University of Toronto, Toronto, ONT, M5S 2S2, Canada

ARTICLE INFO

Article history:
Received 22 October 2020
Received in revised form
8 March 2021
Accepted 8 March 2021
Available online xxx

Handling Editor: Giovanni Zanchetta

Keywords:
Oldowan
Acheulean
Kalahari
African Quaternary
Pleistocene chronology

ABSTRACT

Cave sediments pose dating challenges due to complex depositional and post-depositional processes that operate during their transport and accumulation. Here, we confront these challenges and investigate the stratified sedimentary sequence from Wonderwerk Cave, which is a key site for the Earlier Stone Age (ESA) in Southern Africa. The precise ages of the Wonderwerk sediments are crucial for our understanding of the timing of critical events in hominin biological and cultural evolution in the region, and its correlation with the global paleontological and archaeological records. We report new constraints for the Wonderwerk ESA chronology based on magnetostratigraphy, with 178 samples passing our rigorous selection criteria, and fourteen cosmogenic burial ages. We identify a previously unrecognized reversal within the Acheulean sequence attributed to the base of the Jaramillo (1.07 Ma) or Cobb Mtn. subchrons (1.22 Ma). This reversal sets an early age constraint for the onset of the Acheulean, and supports the assignment of the basal stratum to the Olduvai subchron (1.77–1.93 Ma). This temporal framework offers strong evidence for the early establishment of the Oldowan and associated hominins in Southern Africa. Notably, we found that cosmogenic burial ages of sediments older than 1 Ma are underestimated due to changes in the inherited $^{26}Al/^{10}Be$ ratio of the quartz particles entering the cave. Back calculation of the inherited $^{26}Al/^{10}Be$ ratios using magnetostratigraphic constraints reveals a decrease in the $^{26}Al/^{10}Be$ ratio of the Kalahari sands with time. These results imply rapid aeolian transport in the Kalahari during the early Pleistocene which slowed during the Middle Pleistocene and enabled prolonged and deeper burial of sand while transported across the Kalahari Basin.

1. Introduction

Southern Africa has a rich fossil and archaeological record. The precise ages of archaeological bearing deposits in South Africa are crucial for our understanding of the timing of critical events in hominin biological and cultural evolution in the region (Woodborne, 2016), and its correlation with the global paleontological and archaeological record. However, methodological constraints of the currently available chronological data limit our ability to construct a robust chronological framework for human evolution in the region. Previous chronometric studies have employed various dating techniques, including magnetostratigraphy (Herries et al., 2009; Mcfadden et al., 1979; Thackeray et al., 2002), cosmogenic burial dating of sediments and artifacts (Gibbon et al., 2009, 2014; Granger et al., 2015), electron spin resonance dating of tooth enamel (Dirks et al., 2017; Grun et al., 1996; Porat et al., 2010) and U-Th or U-Pb dating of tooth enamel and flowstone (Albarede et al., 2006; Dirks et al., 2017; Pickering et al., 2010, 2011). Here, we focus on the Earlier Stone Age (ESA) section in Excavation 1 at Wonderwerk Cave and integrate magnetostratigraphy and cosmogenic burial dating in an attempt to better constrain the South African ESA chronology.

* Corresponding author.
E-mail address: ron.shaar@mail.huji.ac.il (R. Shaar).

https://doi.org/10.1016/j.quascirev.2021.106907
0277-3791/

Wonderwerk Cave, a 140 m long phreatic tube located in the eastern flanks of the Kuruman Hills, between the towns of Danielskuil and Kuruman (Fig. 1A), is a site with unique potential for developing a chronometric baseline for archaeological industries in the region. Although Wonderwerk Cave lacks hominin fossils, its Pleistocene deposits include both faunal and botanical remains as well as archaeological material in a stratified cave fill that spans the Oldowan through a developed Acheulean (Chazan et al., 2008, 2012). The primary context of the Wonderwerk Cave lithic and faunal materials (Goldberg et al., 2015), contrasts with many of the rich Cradle of Humankind paleontological localities (Fig. 1A), which are interpreted as doline infills in which artifacts and fossils are in secondary contexts (Dirks and Berger, 2013; Partridge and Maud, 2000). Since finds at Wonderwerk Cave are *in situ*, they provide a clear and ordered framework to investigate the association of artifacts and ecofacts with age determinations. Within the Wonderwerk sequence we can identify the earliest intentional occupation of a cave associated with Oldowan tools (Chazan et al., 2012), as well as onset of technological innovations including biface manufacture and the elaboration of biface forming (Chazan, 2015). Adding to the significance of the site is the identification of the use of fire in the early Acheulean strata (Berna et al., 2012). Critically, fixing the age of the Oldowan at Wonderwerk Cave provides a means of resolving debates about the timing of this industry and related hominin species in Southern Africa.

Previous chronometric efforts at Wonderwerk Cave have included radiocarbon for the uppermost levels (Ecker et al., 2017); optically stimulated luminescence (OSL) for horizons younger than ~0.3 Ma (Chazan et al., 2008, 2020); cosmogenic burial ages for sediments older than ~0.5 Ma (Chazan et al., 2008, 2012; Matmon et al., 2012), magnetostratigraphy (Chazan et al., 2008, 2012; Matmon et al., 2012); U-Th dating (Beaumont and Vogel, 2006) and U-Pb dating (Pickering, 2015) of buried stalagmites younger or older than ~0.3 Ma, respectively. Here we present new paleomagnetic data and cosmogenic burial dates and compare the new results with former chronostratigraphic constraints with specific

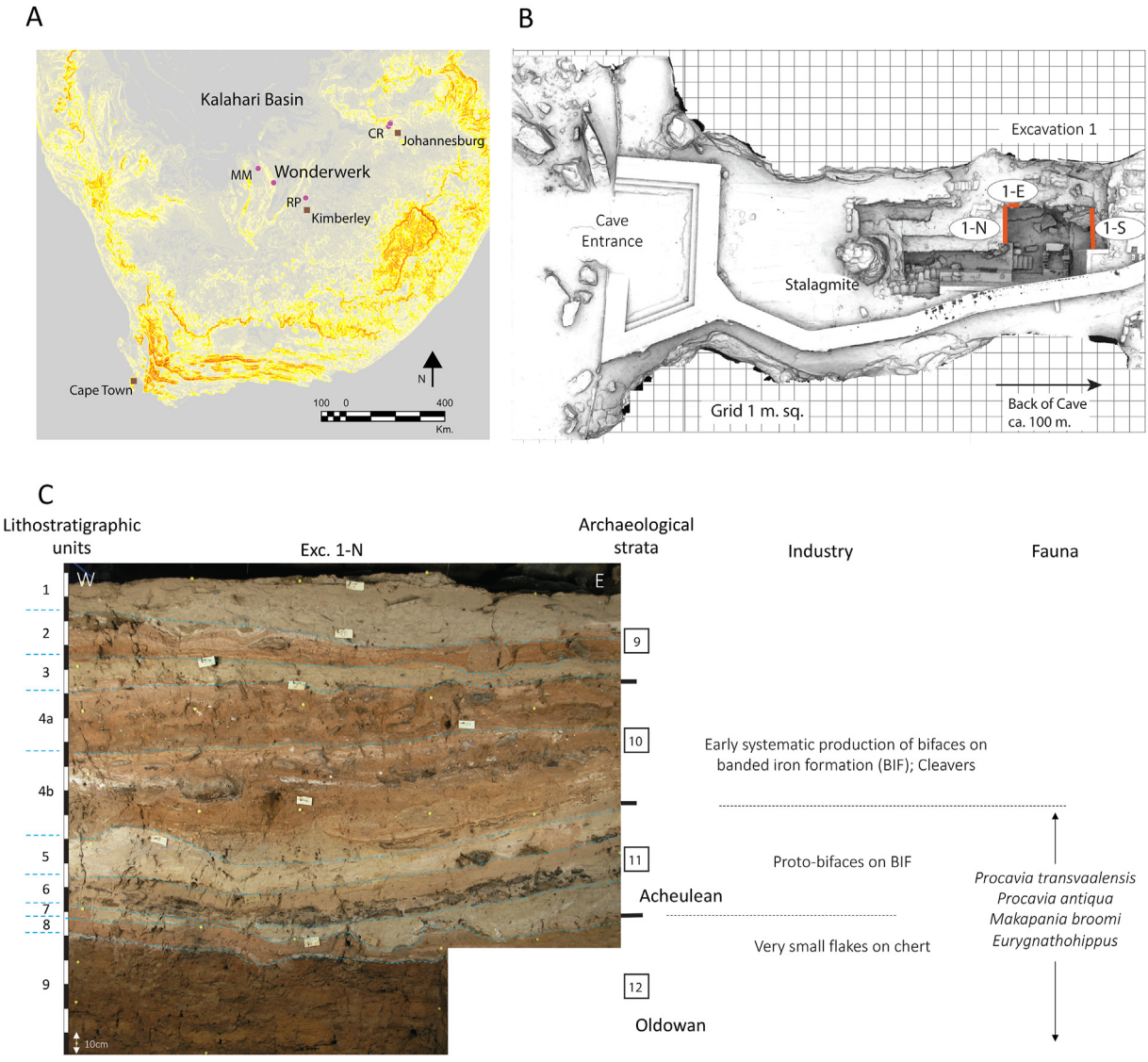

Fig. 1. Location maps and cave section description. A) Terrain slope map showing location of Wonderwerk Cave and other sites mentioned in the text. MM = Mamatwan, RP = Rietputs Formation, CR = sites in the Cradle of Humankind (Sterkfontein, Swartkrans, Malapa, Cooper's, Kromdraai). B) 3D model of Excavation 1 at Wonderwerk Cave (courtesy Zamani project, University of Cape Town) with red lines demarcating the position of the three dated sections: North (Exc. 1-N), East (Exc. 1-E) and South (Exc 1-S). C) Photograph of the North section (Exc. 1-N) showing: lithostratigraphic units (denoted by broken blue lines), archaeological strata and sort description of salient technological features and fauna associated with each archaeological stratum. (For interpretation of the references to colour in this figure legend, the reader is referred to the Web version of this article.)

aims to: 1) test the age of the basal archaeological deposits and the associated Oldowan lithic industry, 2) refine the magnetostratigraphy of the Acheulean strata, and 3) explore processes associated with sediment deposition in the cave and the corresponding cosmogenic burial ages.

2. Sampled section

2.1. Geological and archaeological stratigraphy

Samples for this study were collected from two profiles which were excavated between the 1970s and the early 1980s by Peter Beaumont (Fig. 1) (Beaumont and Vogel, 2006; Horwitz and Chazan, 2015). Both sections are located in Excavation 1 (hereafter Exc. 1), which lies ca. 30m in from the cave entrance (Fig. 1B). The North profile, termed hereafter Exc. 1-N, is along the 28/29 grid line (the original grid was established by Beaumont in yards). The South profile (Exc. 1-S) is six yards (5.48m) to the south along the 34/35 grid line. Beaumont excavated Exc. 1 in archaeological strata (hereafter St., Fig. 1C). St. 12-6 correspond to the ESA deposits and St. 5 is transitional between the ESA and the Later Stone Age (LSA), which is represented in the overlying St. 4-1. Middle Stone Age (MSA) deposits have not been identified in Exc. 1 but occur in the adjacent Exc. 2 (Chazan et al., 2020).

In Exc. 1-N, the basal St. 12 is associated with an Oldowan industry characterized by very small flakes and cores on chert nodules (Chazan et al., 2012). The overlying St. 11 has a very small lithic assemblage that includes two poorly formed bifaces made on banded iron formation (BIF). St. 10-8 provide evidence of the systematic production of handaxes with non-invasive flake removals and relatively low refinement index (length/thickness), most manufactured on BIF (Chazan, 2015). In St. 7-6 there is a shift to more invasive shaping of bifaces resulting in a higher refinement index. In these levels, there are also some forms, particularly well-made sidescrapers, that might indicate a connection to the transitional ESA/MSA Fauresmith industry. The archaeological assemblage at Wonderwerk thus spans the entire ESA from the Oldowan, through the initial appearance of handaxes, to their refinement. However, the total sample size is small and based on the sedimentological evidence it is clear that this is not a continuous depositional record (Goldberg et al., 2015). For previous dating of the Exc.1-N see Chazan et al. (2012); Chazan et al. (2008); Matmon et al. (2012) (note that in Chazan (2015) the North profile is erroneously placed along the 25/26 gridline).

Based on field observations, micromorphology, and Fourier transform infrared (FTIR) spectroscopy, the ESA Exc. 1-N sequence was divided by Goldberg et al. (2015) into ten lithostratigraphic units (Fig. 1C). The basal Unit 10 (underlying St. 12) is described as bedded silts and clay. Unit 10 was not dated since it formed before the cave was accessible to hominins and so falls outside the scope of the archaeological research. The contact between Unit 10 and the overlying Unit 9 is sharp. Unit 9 (equivalent in part to St. 12), is the only component that shows clear signs of water deposition (defined as low energy sheet flow), with finely laminated sand and silt. It also includes bedding of sub-angular, cm-sized clasts of ironstone and altered dolomite. However, even in this stratum, there is no indication of any high energy water transport capable of transporting artifacts and faunal material from the outside of the cave into Exc. 1 that is located far from the cave entrance (Goldberg et al., 2015). Thus, the artifacts and fauna were deposited synchronously within the sediment, and the dates obtained provide an age for these stratigraphically associated finds. Units 8-1 are all aeolian in origin and include an important component of silty clay aggregates that are interpreted as evidence of a temporary pan or basin near the cave mouth. There is regular evidence for erosional events and discontinuities in deposition. Depositional hiatuses were observed based on the presence of sharp or erosional contacts between units, and are described in detail in Goldberg et al. (2015). Fragments of dolomite roof fall are abundant in Units 2, 4b, and 6-8, indicating that rockfall plays a role in the depositional sequence. The base of the southern section in Exc. 1 (Exc. 1-S, Fig. 1B) corresponds to the lithostratigraphic units documented in Exc.1-N. However, the upper deposits of the Exc. 1-S ESA sequence (corresponding to St. 8-6) dip southward and therefore appear in this section but are not included in the lithostratigraphy of Exc. 1-N presented in Fig. 1C (Goldberg et al., 2015).

2.2. Fauna

Fauna from St. 12 and 11 include three extinct taxa that are characteristic of the Makapanian Land Mammal Stage (LMS) dated to ~2.8 to ~1.5 Ma (Brink et al., 2016), that spans part of the newly defined Shunguran and Natrorian LMS (Van Couvering and Delson, 2020). They include two species of fossil hyrax - *Procavia transvaalensis, Procavia antiqua,* and a large caprine with similarities to, although larger than, *Makapania broomi.* The presence of a large-sized caprine is known from Makapan Limeworks Members 3 and 4, both dated to <2.6 Ma, as well as from Kromdraai B, Swartkrans Member 1 and the basal levels at Olduvai (Kenya) dated to ~2 Ma (Fourvel et al., 2016; Gentry, 2010). The Makapan Limeworks caprine specimen is the most similar in terms of size to the specimen found in Wonderwerk Cave (Brink et al., 2016). The two extinct species of *Procavia* found in both Wonderwerk St. 12 and 11, are components of other Makapanian LMS deposits in Southern Africa - such as Makapan Limeworks, Taung, Bolt's Farm, Cooper's, Swartkrans, Sterkfontein and Kromdraai (Rasmussen and Gutiérrez, 2010). Notably, these extinct forms of hyrax are absent in the other ESA levels at Wonderwerk. Hipparion (*Eurygnathohippus*), occurs in both St. 12 and 11, but became extinct in the region as late as ~1.0 Ma (Brink et al., 2016). Hipparions occur in other Makapanian LMS sites such as Swartkrans Member 1, Kromdraai A and possibly the older deposits at Gladysvale. Together, these findings confirm the antiquity of St. 12 and 11 at Wonderwerk (Brink et al., 2016). Aside from *Hystrix africaeaustralis*, other fauna from these layers at the cave could only be identified to the level of Family, and so are of limited use for biochronological attribution.

3. Methods

3.1. Paleomagnetic stratigraphy

Paleomagnetic sampling of Exc. 1 was carried out during excavation seasons 2005, 2007, 2016 and 2018. The pre-2016 data included 87 samples from Exc. 1-N and Exc. 1-E, the perpendicular abutting profile to the east of Exc. 1-N (Fig. 1B). These were used to construct an initial magnetostratigraphic age model (Chazan et al., 2008, 2012; Matmon et al., 2012). During seasons 2016 and 2018 we collected additional 282 samples: 226 samples from Exc. 1-N and 56 samples from Exc. 1-S. Paleomagnetic sampling was undertaken either using non-magnetic plastic boxes ($1.5 \times 1.5 \times 2$ cm) for Alternating Field (AF) demagnetization procedures, or using quartz cylindrical crucibles, 2.54 cm (1") in diameter and height, for thermal demagnetization. When using plastic boxes, a cube-shaped sample with three vertical faces and two horizontal faces was carved from the section that had been cut back a few centimeters to create a fresh face. The sediment sample was then placed in the plastic box and its orientation was precisely measured using a Brunton compass. After detaching the sample from the section, the

sediment was glued in the box using non-magnetic potassium silicate glue. A similar sampling technique was used for the quartz cylinders. The x,y,z coordinates of each sample was recorded using a total station. The magnetic azimuths were corrected for declination using IGRF model (Thebault et al., 2015).

Paleomagnetic experiments were carried out at the paleomagnetic laboratory in the Institute of Earth Sciences, the Hebrew University of Jerusalem using two superconducting rock magnetometers (SRM): a single-specimen 2G-750 and a multi-specimen 2G-RAPID, each equipped with in-line 2-axis AF demagnetization coils. Thermal demagnetizations were carried out using an ASC-TD48 thermal demagnetizer. AF demagnetizations were done at progressively elevated peak magnetic fields, in 5 mT or 10 mT steps, up to 110 mT. Thermal demagnetizations were carried out in 50 °C steps from 50 °C up to 200 °C, and then in 40 °C, 30 °C, or 20 °C steps up to 700 °C, or until the samples were completely demagnetized. In total, 216 samples were demagnetized using AF and 66 samples were demagnetized thermally. Thermomagnetic curves and susceptibility measurement were measured using an AGICO MFK-1 Kappabridge equipped with CS4 furnace. Isothermal remanent magnetizations (IRM) were imparted using ASC pulse magnetizer and measured using MAG-Instruments PSM-1 spinner. IRM were done in a 1.4 T field and in a −0.3 T backfield. S-ratio (Liu et al., 2012) is defined here as: $S = 0.5 \times \left(1 - \frac{IRM_{-0.3\ T}}{IRM_{1.4\ T}}\right)$, where values close to 1 indicate the dominance of low coercivity minerals and values close to 0 indicate the dominance of high coercivity minerals.

All new paleomagnetic data, as well as legacy data from Exc.1-N, were translated to the community standard MagIC format (Tauxe et al., 2016). These data also include the total station coordinates of the samples. The entire dataset was interpreted using the Demag-GUI program, a part of the PmagPy software package (Tauxe et al., 2016). The direction of the characteristic remanence magnetization was calculated from the orthogonal end-point Zijderveld diagrams (Zijderveld, 1967) using principle component analysis (Kirschvink, 1980). The raw paleomagnetic measurement data as well as the interpretations and results are available in the publicly accessible MagIC database (https://www2.earthref.org/MagIC/16774).

3.2. Cosmogenic isotope burial dating

Cosmogenic isotope burial dating enables the dating of sediments over a time range of 0.3–5 Ma (Granger, 2006; Granger and Muzikar, 2001; Hidy et al., 2014; Matmon et al., 2014). ^{10}Be-^{26}Al burial dating of sediment is based on a process in which these two nuclides are produced in a material at, or near, the surface at a known ratio, and then buried and shielded from further cosmic-ray bombardment such that production effectively ceases. Once production is shut off, nuclide concentrations are governed by radioactive decay. The concentration ratio ^{26}Al/^{10}Be decreases with time since ^{26}Al decays about twice as fast as ^{10}Be: the half-life of ^{10}Be is 1.387 Ma (Chmeleff et al., 2010; Korschinek et al., 2010) and the half-life of ^{26}Al is 0.705 Ma (Nishiizumi, 2004). A simple burial age is calculated from the ratio of ^{26}Al and ^{10}Be concentrations following Granger et al. (1997): $\left(\frac{N_{26}}{N_{10}}\right)_{(t)} = \left(\frac{N_{26}}{N_{10}}\right)_{(0)} e^{-t_{burial}\left(\frac{1}{\tau_{26}} - \frac{1}{\tau_{10}}\right)}$, where $\left(\frac{N_{26}}{N_{10}}\right)_{(t)}$ is the ratio of the measured ^{26}Al and ^{10}Be concentrations, $\left(\frac{N_{26}}{N_{10}}\right)_{(0)}$ is the initial ^{26}Al to ^{10}Be concentrations at the time of burial, t_{burial} is the time since burial, and τ_{10} and τ_{26} are the mean lives of ^{10}Be and ^{26}Al, respectively (Granger and Muzikar, 2001). The ratio $\left(\frac{N_{26}}{N_{10}}\right)_{(0)}$ can be determined from the accepted surface production ratio of ^{26}Al and ^{10}Be in quartz. In most natural settings this value is ~6.8 (Balco et al., 2008; Nishiizumi et al., 2007), although some studies suggest that the ratio may vary slightly with altitude (Argento et al., 2013; Lifton et al., 2014) and lower ratios will develop after long and continuous exposure periods (>300ka) or due to very slow erosion rates (<10 m/Ma). Complications to the simple age calculation arise if the pre-burial ratio is below that of the production ratio (for example, if there was a previous burial period or if bedrock was exhumed very slowly), or if burial was shallow such that post-burial nuclide production by deeply penetrating muons still occurred. In these cases, either a maximum or minimum age for the case of a significant inherited depositional ratio or post-burial production, respectively, is given, or additional independent constraints are required.

^{10}Be-^{26}Al burial dating methods can generally be applied to sediments that are buried longer than 0.3 Ma, at which time the measured ^{26}Al/^{10}Be ratio can be reliably distinguished from the surface production ratio. The maximum limit of the method is ~5 Ma, at which time ~7 half-lives of ^{26}Al reduce its concentration either to secular equilibrium, which is controlled by the very low production rate of nuclides by deeply penetrating muons, or to a level beneath current AMS measurement (Matmon et al., 2014).

Fourteen samples were collected from Exc. 1-N for cosmogenic burial dating. These include seven previously published samples (Matmon et al., 2012) and seven new samples. Measurements of ^{10}Be and ^{26}Al were made on quartz 60–250 μm grain-size fraction. Quartz cleaning procedure and the extraction of Be and Al cations (converted to oxides) followed the procedures described in Kohl and Nishiizumi (1992) and Bierman and Caffee (2001). Samples were analyzed at the AMS facilities of ASTER (CEREGE, Aix en Provence, France) and LLNL (Livermore, California). Isotopic ratios of ^{10}Be/Be and ^{26}Al/Al were corrected with chemistry processed blanks and normalized to accepted in-house AMS Standard Reference Materials with agreed nominal isotopic ratios.

The initial pre-burial ^{26}Al/^{10}Be concentrations ratio was estimated from measurements of four exposed surface-sand samples collected outside the cave. These include two samples collected from a surface ca. 3 km from the Cave and analyzed twice at two different occasions (COS-SUR; COS-SUR(rep)) and two sand samples from the surface of the Kalahari Desert, ~70 km north of the cave (Sand 13 and Sand 14). Detailed descriptions of these samples are given in Matmon et al. (2015); Matmon et al. (2012).

Rock shielding in the cave was estimated using trigonometric calculations considering the angle of the slope above the cave and the distance of the site from the mouth of the cave, and later confirmed from detailed LiDAR mapping of the cave and its surroundings (Matmon et al., 2012; Ruther et al., 2009). The rock thickness in front of the cave above Exc. 1 is 15 m (ρ = ~2.7 g/cm^3). Calculation shows that under such shielding over a time span of 0.5–2 Ma, muogenic production results in 1–8% of the measured ^{26}Al and ^{10}Be concentrations. Given that its impact on cosmogenic burial age calculation is negligible, post burial production has not been considered in our age calculations.

4. Results

4.1. Paleomagnetic results

4.1.1. Magnetostratigraphy

Fig. 2 shows representative demagnetization results of paleomagnetic samples with nearly ideal behaviors, from which an

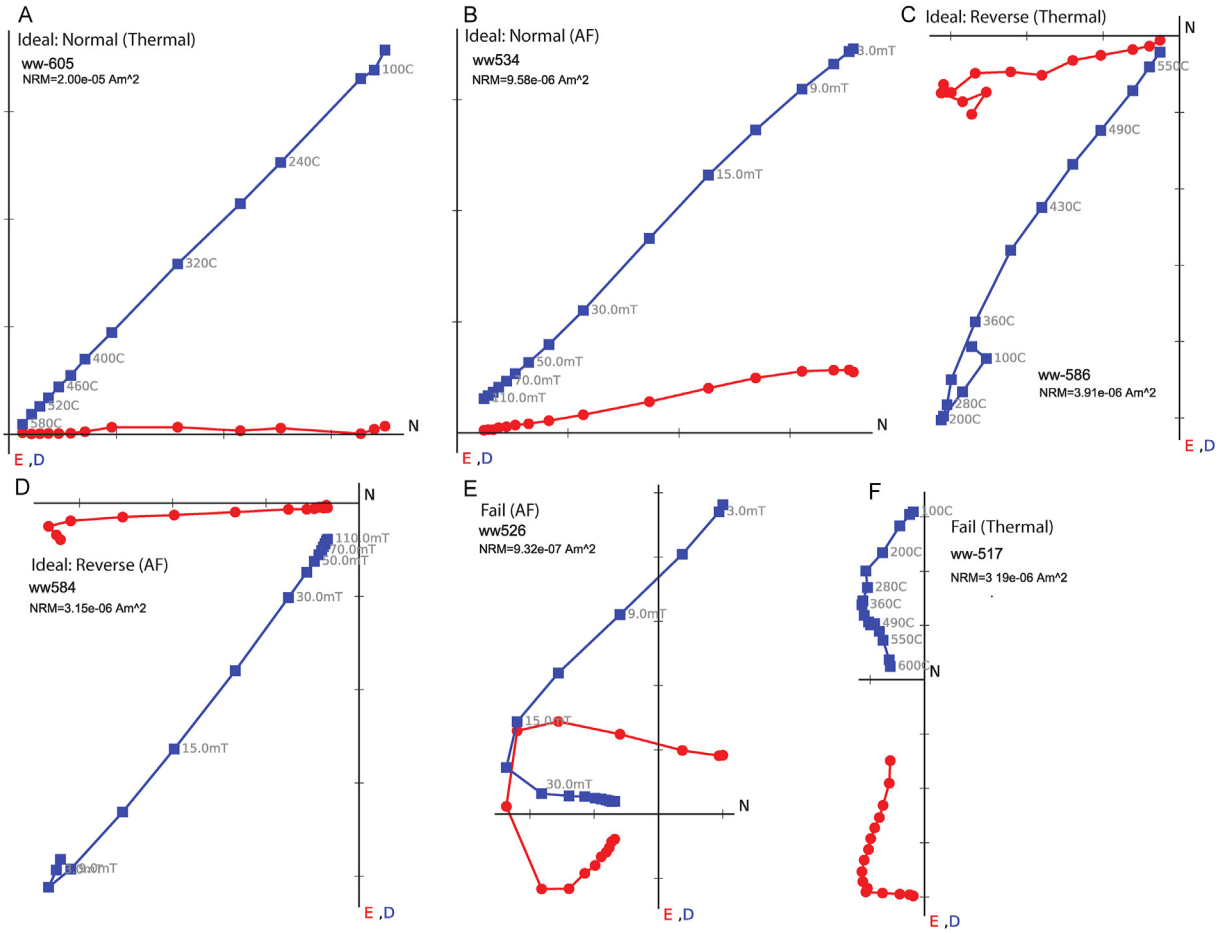

Fig. 2. Representative demagnetization data. Data are shown as Zijderveld end-point orthogonal plots (Zijderveld, 1967) with red squares and blue circles representing projection of the magnetization vector on the north-east and north-down planes, respectively. A-B) Normal polarity passing acceptance criteria. C-D) Reverse polarity passing acceptance criteria. E-F) Examples of specimens failing acceptance criteria (see text for details). Demagnetization steps are noted near symbols. (For interpretation of the references to colour in this figure legend, the reader is referred to the Web version of this article.)

unambiguous polarity state can be inferred, as well as results failing to provide a robust paleomagnetic direction. An ideal behavior is characterized by a univectorial magnetization pointing northward and upward (declination near zero and negative inclination) or southward and downward (declination near 180 and positive inclination), for normal and reverse polarity, respectively. This is visually expressed as straight end-point Zijderveld plots (Zijderveld, 1967) converging toward the origin (i.e. Fig. 2A–D). Examples of Zijderveld plots from which we cannot obtain reliable paleomagnetic interpretations are shown in Fig. 2 E-F. Our criteria for accepting paleomagnetic data are: i) Maximal angular deviation (MAD) (Kirschvink, 1980) $< 15°$, ii) Deviation ANGle (DANG) (Tauxe and Staudigel, 2004) $< 30°$, and iii) The angle between the paleomagnetic direction and the geocentric axial dipole (GAD) direction (declination $= 0°,180°$; inclination $= -46.6°,46.6°$) $< 45°$. The first two criteria assess the scatter of the of the data points about the best fit line and the convergence of the best fit line toward the origin. The third criterion checks if the paleomagnetic direction is in agreement with the expected behavior of the geomagnetic field, where 'normal' and 'reverse' polarities are attributed to paleomagnetic directions falling within a 45° cone around the GAD directions. Other directions may represent sediment re-working by bioturbation or by other physical mixing or alternately, unstable magnetic mineralogy.

From a total of 323 samples analyzed in this study, 178 samples passed the acceptance criteria, 145 of which were demagnetized using AF, and 33 were demagnetized thermally. Out of the rejected samples, only 27 failed the MAD or the DANG criteria. This suggests that post-depositional physical disturbance of the sediments is not uncommon; perhaps part of the sediment was reworked, maybe during the erosional events or as a result of roof falls as reported in Goldberg et al. (2015). The Fisher mean of the entire dataset, when all data are transferred to the same polarity, is: declination $= 357.0$, inclination $= -50.4$, $\alpha_{95} = 2.9$, $k = 14$, $n = 178$, in agreement with the GAD direction, supporting the overall reliability of the accepted results.

Fig. 3A and B shows the paleomagnetic interpretations superimposed on photographs of Exc. 1-N and Exc. 1-S taken during the 2016 and 2018 excavation seasons, respectively. The notations "N" and "R" denote normal and reverse polarity, whereby the notation "?" is used to mark samples failing acceptance criteria. Thirty samples from St. 9-10 (Lithostratigraphic Units 4a and 3) in the eastern section of Exc. 1 (Exc. 1-E, Fig. 1B), previously reported and interpreted as normal polarity (Chazan et al., 2008, 2012) are not shown for clarity. Depth plots showing the declination, inclination, and the virtual geomagnetic pole (VGP) latitude of the data are shown in Fig. 4.

Two clear thick polarity intervals in Exc. 1-N can be clearly identified in Figs. 3-4: a normal interval spanning from the top of the section toward the lower levels of St. 10 (Units 1-4a and the

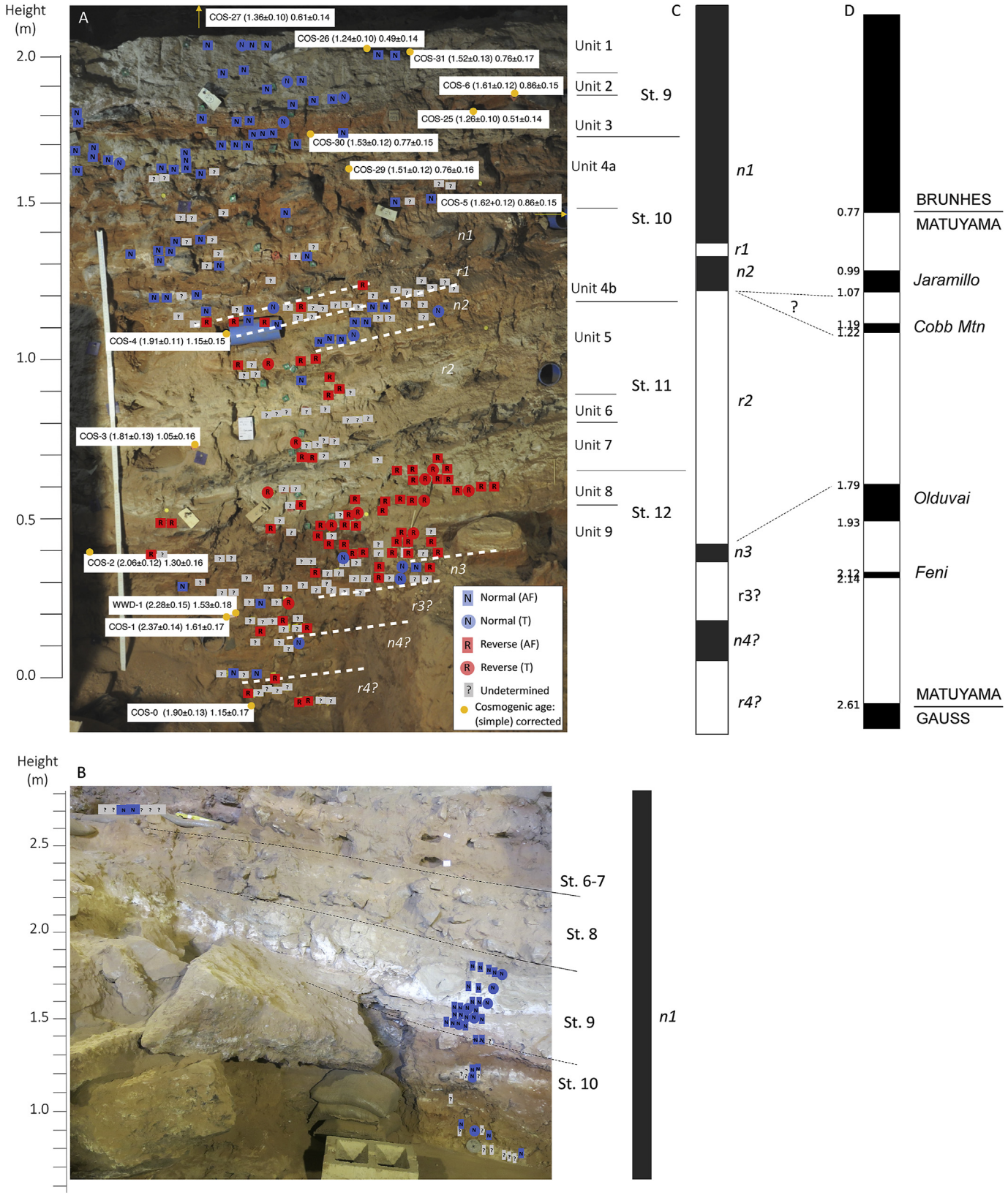

Fig. 3. Magnetostratigraphy and cosmogenic ages. A) Paleomagnetic interpretations and cosmogenic ages superimposed on a photograph of Exc. 1-N taken during the 2016 excavation season. Note that COS-7 is located above the photographed section and COS-5 is located in Exc. 1-E. B) Paleomagnetic interpretations of Exc1-S superimposed on a photograph taken during the 2018 excavation season. Blue (red) symbols denote for normal (reverse) samples; squares and circles are AF and thermal demagnetizations, respectively. Dashed white lines in (A) mark boundaries between magnetostratigraphic intervals. The boundaries between archaeological strata and the lithostratigraphic units are shown to the right of figures. C) Magnetostratigraphy of Exc. 1-N with division to magnetic polarity intervals. D) Correlation to the geomagnetic polarity time scale. (For interpretation of the references to colour in this figure legend, the reader is referred to the Web version of this article.)

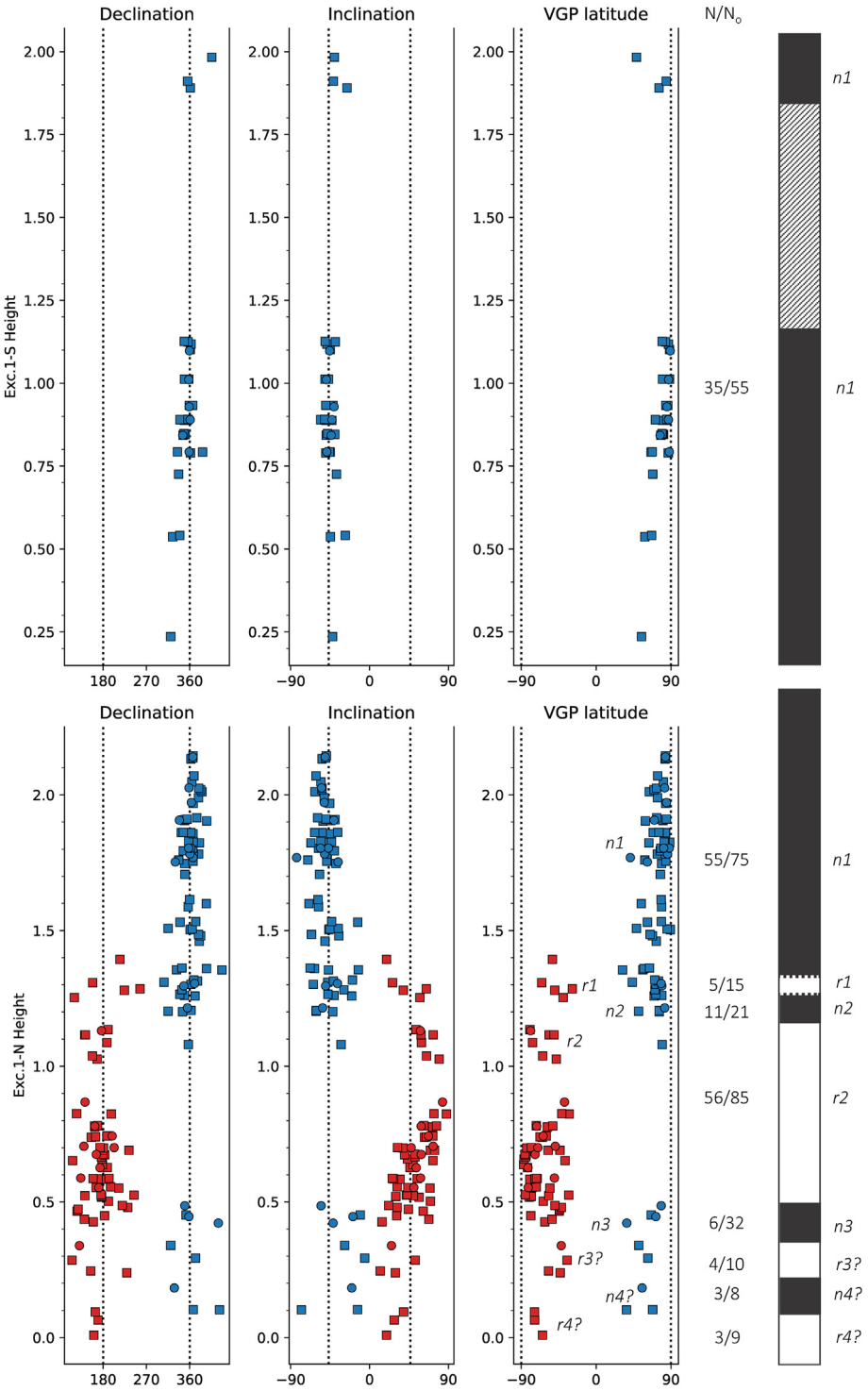

Fig. 4. Paleomagnetic depth plot. Top (bottom) panel shows declination, inclination, and VGP latitude of Exc.1-S (Exc 1-N). Squares and circles represent AF and thermal samples, respectively. Blue and red denote normal and reverse polarity, respectively. The magnetostratigraphic intervals are shown in the right. Some overlaps of the magnetic polarity intervals are apparent owing to the westward dip of the sedimentary layers (see Fig. 3). N/N_0 denotes the number of samples passing criteria versus all samples in the polarity interval. (For interpretation of the references to colour in this figure legend, the reader is referred to the Web version of this article.)

upper part of Unit 4b): *n1* in Fig. 3A,C; a reverse interval spanning from the top of St. 11 through the upper parts of St. 12 (Unit 5 through the upper part of Unit 9): *r2* in Fig. 3A,C. The zone separating these two intervals (lower part of Unit 4b) includes a mixed interval with a thin dipping horizon, a few cm in thickness, with five reverse AF samples (*r1*), bracketed by the overlying *n1* and by an underlying 10 cm thick normal polarity horizon (*n2*). An enlarged picture of horizon *r1* and the Zijderveld plots of the reverse samples in *r1* are shown in Fig. 5. While there are only five reverse samples in *r1*, we interpret *r1* as a reverse layer because in order to record a reverse direction, the sediment must have been subjected to a reverse field at some point since deposition. As noted

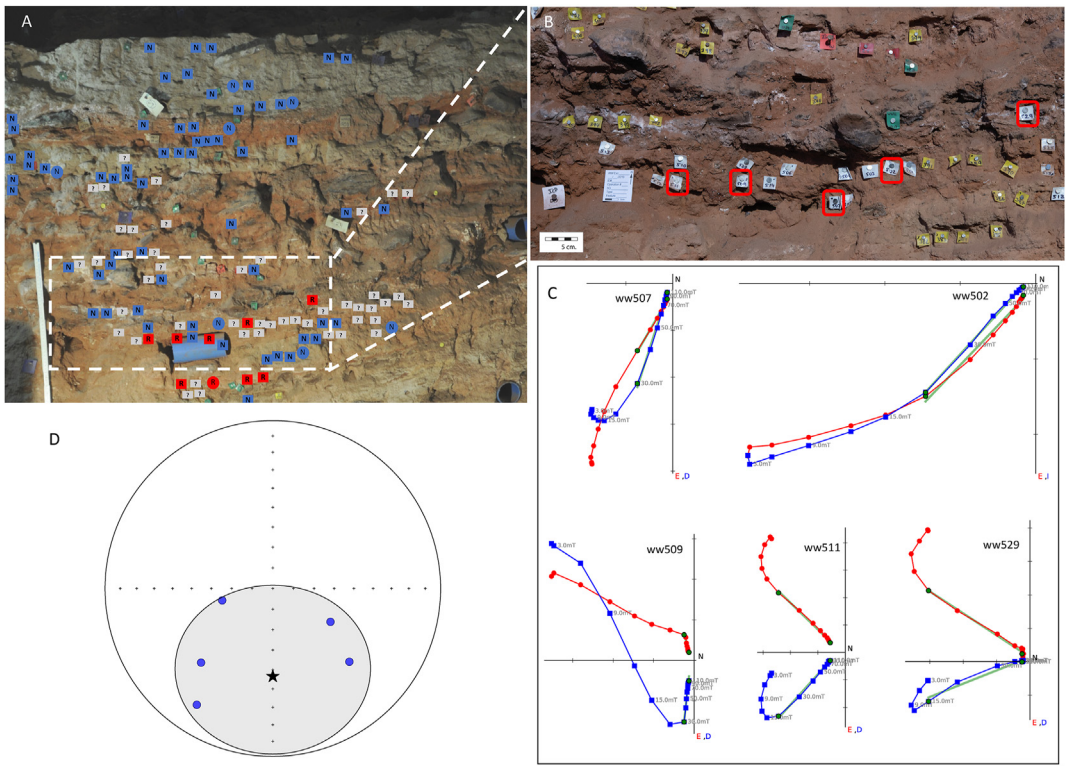

Fig. 5. Reverse horizon *r1*, separating between *n1* and *n2*. A) Photograph of Exc.1-N showing *n1-r1-n2* transitions. Blue and red symbols mark normal and reverse samples, respectively. B) Magnification of *r1* – a dipping thin silty layer with five reverse AF samples (marked with red frame). C) Zijderveld plots (see Fig. 2) showing the demagnetization results of the reverse samples shown in (B). Green lines show the least square best fit line. D) Equal area projection showing the expected reverse field direction (star) and 45° cone around it (filled area). Blue circles show the direction of the samples in B-C. (For interpretation of the references to colour in this figure legend, the reader is referred to the Web version of this article.)

in Goldberg et al. (2015), Unit 4b is characterized by disconformity and large clasts of dolomite originating from roof fall. Thus, the most likely scenario is that *r1* was deposited during a reverse polarity interval, but complicated sedimentation processes and possibly hiatuses led to the complexity of the mixed zone of *r1* and *n2* and low success rate in the paleomagnetic analysis.

The lowest part of Exc. 1-N below *r2* is mixed with both normal and reverse samples. A careful inspection of this interval raises the possibility that there are two normal layers, and two reverse layers. The top layers (*n3 – r3? – n4?*) are supported by both AF and thermal data and the lowermost reverse one is supported only by AF data. Given the uncertainty associated with this zone, we mark *r3?* and *n4?* in Fig. 3 and elsewhere with a question mark.

The uppermost levels (St. 6-7) in Exc. 1-S (Fig. 3B) consist of only normal polarity samples. St. 8 could not be sampled because of the large number of dolomite clasts, leading to a gap in the magnetostratigraphic sequence. All underlying samples in Exc. 1-S corresponding to St. 9-10, are normal polarity and attributed to interval *n1*.

4.1.2. Rock magnetism

Fig. 6A shows thermomagnetic heating curves of representative samples from all stratigraphic units. All units show maximum Curie temperatures exceeding the Curie temperature of magnetite (580 °C), between 600 °C and 650 °C. In addition, the susceptibility of some samples starts decaying between 350 °C and 500 °C, and at Unit 7 there is a significant decrease in susceptibility at temperatures below 300 °C. The decay of the normalized magnetizations in the thermal demagnetization experiments, calculated using the vector difference sum (VDS) (Tauxe et al., 2018) are shown in Fig. 6B for the specimens that passed criteria. Many samples are nearly entirely demagnetized at 580 °C, at the Curie temperature of magnetite, while other are demagnetized only at 680 °C. The median destructive temperatures (MDT), calculated from the data shown in Fig. 6B, range between 200 °C and 600 °C (Fig. 6C). To further examine the magnetic mineralogy in Exc. 1-N, we show in Fig. 7, depth plots of the MDT, median destructive fields (MDF), and S-ratio. Here, we see that the MDF in nearly all samples is 10–30 mT, with only 12 samples having MDF >40 mT (at the boundary between St. 12 and St. 11, and at the boundary between St. 11 and St. 10). Low coercivity is also evident in the S-ratio, which is higher than 0.95 for most of the stratigraphic sequence. Altogether, the combined observations suggest a complex mixture of magnetic mineralogy: the combination of Curie temperature above 580 °C, low coercivity and high S-ratio suggest dominance of maghemite and perhaps partially oxidised magnetite; the drop in thermomagnetic curves between 500 and 600 °C associated with low blocking temperatures, low coercivities and high S-ratio suggests the presence of (titano)magnetite; the low S-ratio in St. 12 suggest also the presence of hematite.

The variations in the magnetic parameters with depth is shown in Fig. 7. Evidently, the magnetic mineralogy is not homogeneous throughout the stratigraphic sequence of Exc. 1. The mass-normalized Isothermal Remanent Magnetization (IRM) and susceptibility are higher in St. 9 and in St. 11 and the S-ratio is significantly lower in St. 12. We note that changes in the magnetic parameters do not correlate with the transitions between magnetostratigraphic units as large changes in the magnetic mineralogy are observed within the thick intervals of *n1* and *r2*. Thus, it seems unlikely that polarity changes are caused, or triggered, by changes

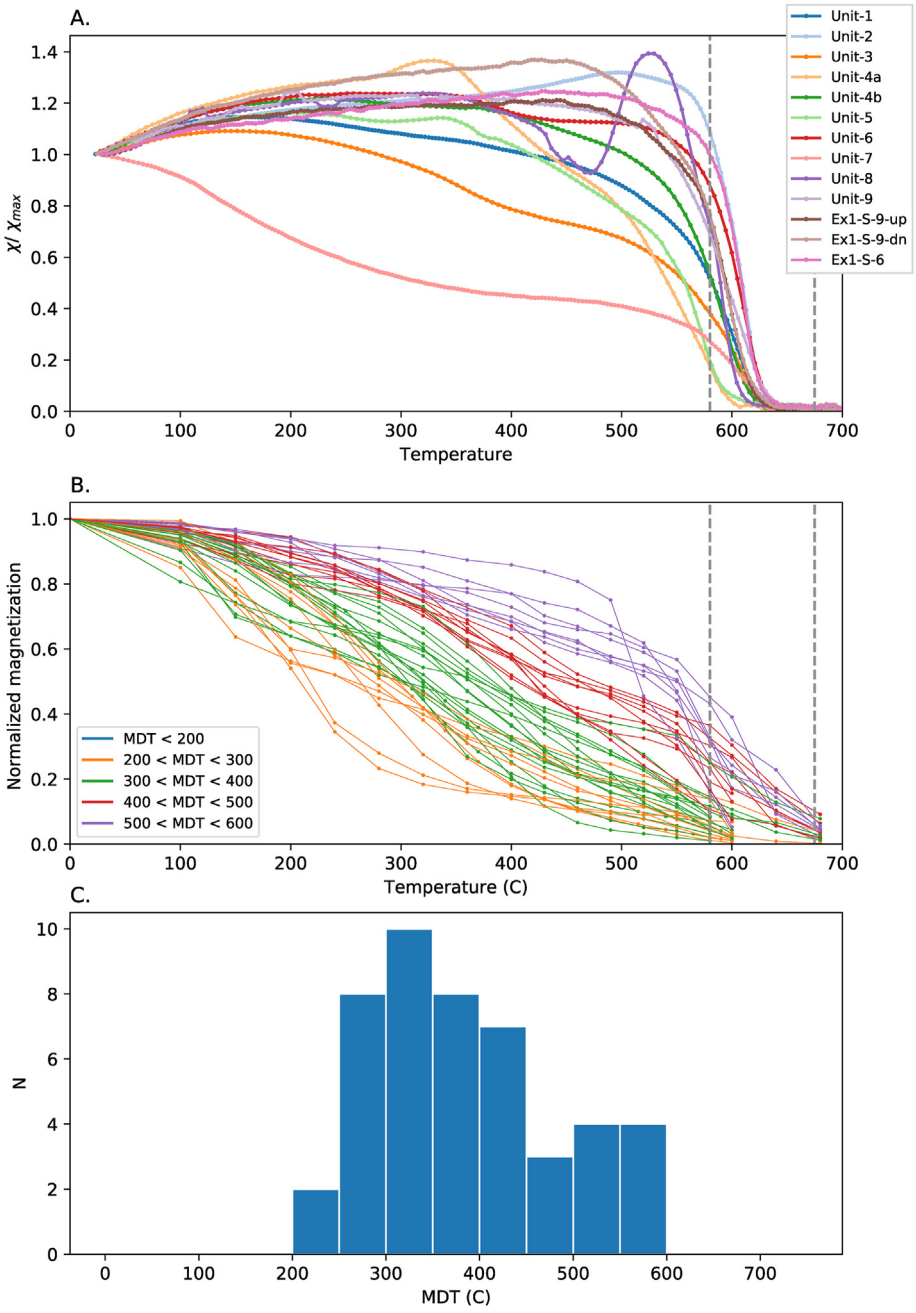

Fig. 6. High temperature magnetic behavior. A) thermomagnetic curves of sediment samples collected from all sedimentary units (Figs. 1 and 3). B) Normalized magnetization versus temperature of samples that passed the criteria. The Curie temperature of magnetite and hematite are marked with dashed vertical lines in (A-B). C) histogram of the median destructive temperature (MDT) of the samples shown in (B).

in the magnetic minerals.

4.2. Cosmogenic burial ages

Table 1 lists cosmogenic burial age data of 14 Wonderwerk Cave samples: seven from this study and seven previously reported in Matmon et al. (2012). ^{10}Be concentration range between $10.8 \pm 0.4 \times 10^5$ atoms g^{-1} quartz and $27.3 \pm 0.6 \times 10^5$ atoms g^{-1} quartz. ^{26}Al concentrations follow a similar pattern to that of ^{10}Be and they range between $20.7 \pm 1.3 \times 10^5$ atoms g^{-1} quartz and $81.1 \pm 3.5 \times 10^5$ atoms g^{-1} quartz. ^{26}Al/^{10}Be ratios range between 1.91 ± 0.13 and 3.12 ± 0.15. Simple burial ages were calculated using the iteration approach of Granger et al. (1997) and range between 2.37 ± 0.14 Ma (COS-1) and 1.24 ± 0.10 Ma (COS-26). Four sand samples, collected from the surface near the cave and from ~70 km north of the cave (see Methods), yielded an average ^{26}Al/^{10}Be ratio of 3.90 ± 0.31 (Table S1, Supplementary Material) (Matmon et al., 2012). This ratio corresponds to a simple burial age of 0.75 ± 0.1 Ma. This depressed ratio, relative to the production rate ratio, results from a complex exposure-burial history of the sands while being transported across the Kalahari Desert (Vainer et al., 2018a, 2018b). Under a simplified assumption that the ^{26}Al/^{10}Be ratio of the sediments entering the cave has remained constant during the past 2 Ma (this assumption is challenged in the Discussion section below), we subtract the apparent initial age of the surface sands from the simple burial ages obtained for the

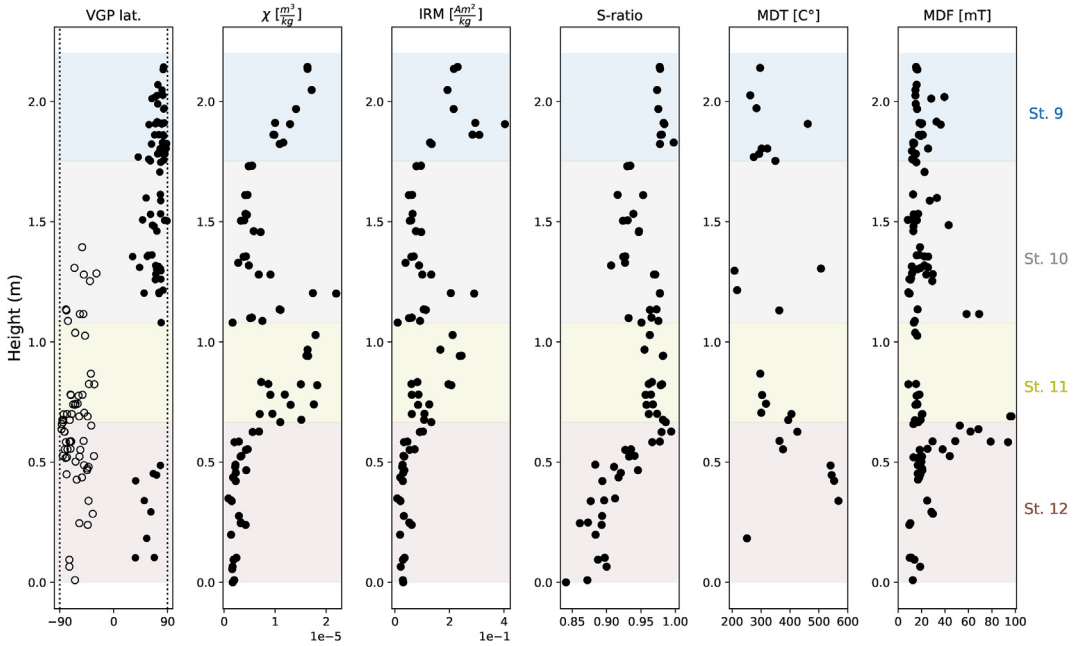

Fig. 7. Virtual Geomagnetic Poles (VGP) and rock magnetic parameters of Exc. 1-N. See text for details.

sediments in the cave. We denote these ages as "corrected ages" in Table 1. Throughout the text we refer to the corrected burial ages when discussing cosmogenic ages unless specified otherwise. The corrected ages range between 1.61 ± 0.17 Ma (COS-1) and 0.49 ± 0.14 Ma (COS-26) (Table 1). Fig. 3A shows the location of 13 samples in the section (the uppermost one was taken from a step located above Exc. 1-N and is not shown in the picture) and their corresponding cosmogenic ages.

Fig. 8A shows the age span of the simple and the corrected ages, where ages are displayed according to their stratigraphic position in the sedimentary sequence. In general, and considering the error bounds, the cosmogenic ages increase with depth, with only two exceptions (COS-25, COS-0). We note that the sampling scheme includes four horizons with two or three samples per horizon (see Methods). In these horizons, the samples yield overlapping burial ages, except sample COS-25.

5. Discussion

5.1. Updated age model of Exc. 1 sequence

The paleomagnetic – cosmogenic age model of Wonderwerk sequence is based on tying the paleomagnetic polarity sequences in Exc. 1–N and Exc. 1–S to the most recent Quaternary geomagnetic polarity timescale (Channell et al., 2020) and to the cosmogenic burial ages (Fig. 3).

The archaeological evidence in St. 7-6 of a shift towards highly refined handaxes (Chazan, 2015) suggests that the upper units are younger than the Brunhes-Matuyama (B-M) boundary (0.77 Ma). Thus, we assign St. 7-6 in Exc. 1-S to the Brunhes Chron (0–0.77 Ma). St. 9-10 in Exc. 1-S and St. 9 to the upper part of St. 10 in Exc. 1-N are clearly normal, and therefore, interval *n1* falls within the Brunhes. The thick normal polarity interval *n1* is underlain by *r1* - a thin horizon at the lower part of St. 10 (in Unit 4b) with five reverse samples. The thickness of *r1* creates a problem to the magnetostratigraphic interpretation because the reverse intervals in the Matuyama are relatively long (Fig. 3D) while the thickness of *r1* is only a few centimeters (Fig. 5). This suggests a hiatus in deposition or an erosional event associated with *r1*. Some corroboration for this is found in the micromorphology which demonstrates a clear distinction between Unit 4b, which at its top comprises centimeter-sized elongated fragments of dolomitic roof spall, while the majority of clasts are slightly to moderately weathered, in contrast to the upper Unit 4a, which comprises rounded calcareous sand with pockets of microfauna. As we attempt the simplest age model with as few and as short hiatuses as possible as a starting point for the initial magnetostratigraphic model, there are several options for the extent of a single hiatus, as shown in Fig. 9. All these options assume that *n2*, which is ~10 cm thick, is either the Jaramillo or the Cobb Mtn. subchron. The latter assumption is justified below based on cosmogenic evidence. Given the slow sedimentation rate, the limited sampling resolution and the possibility of hiatus or erosion, it is likely that one of the short subchrons (Jaramillo, Cobb Mtn.) was not recovered in the magnetostratigraphy. Thus, the *n2-r2* transition can be the base of the Jaramillo or the base of the Cobb Mtn. Below *n2*, St. 11 and the top of St. 12 is a thick reverse interval (*r2*), with one isolated normal sample that we treat as an outlier. This interval best fits with the long reverse interval between Jaramillo/Cobb Mtn. and the Olduvai (1.93–1.77 Ma). Below *r2* there is a mixed zone within St. 12 which yielded both normal and reverse results. While it is difficult to pinpoint the horizons of reversals, it is most likely that the upper normal level in St. 12 is the Olduvai. It is possible that there is a succession of N-R-N-R representing both the Olduvai and the Feni subchron (2.14–2.12 Ma), but this hypothesis is uncertain owing to the relatively low success rate of the paleomagnetic analysis in St. 12, possibly due to bioturbation in these deposits (Goldberg et al., 2015).

We now test the above simple magnetostratigraphic model from different perspectives – cosmogenic burial ages, sedimentation rates and archaeological evidence. Eight cosmogenic burial ages from the top of Exc. 1-N down to COS-5 were included in the *n1* interval associated with the Brunhes chron (Fig. 8A). Considering the age uncertainties, these eight samples are in agreement with the magnetostratigraphy. Nevertheless, the error bounds of samples COS-31, COS-6, COS-30, COS-29 and COS-5 extend toward the

Table 1
Cosmogenic ages.

Name	St.	Qtz. Mass (g)	Be spike[c] (g)	$^{10}Be/^{9}Be$[d] ($\times10^{-14}$)	^{10}Be (10^5 atoms g^{-1} quartz)	Al (10^{18} atoms g^{-1})	$^{26}Al/^{27}Al$[§] ($\times10^{-14}$)	^{26}Al (10^5 atoms g^{-1} quartz)	$^{26}Al/^{10}Be$	Simple age (Ma)	Corrected age (Ma)
COS-0[a]	12	20.018	0.184	182 ± 6	15.6 ± 0.6	2.92	125 ± 4	36.4 ± 1.8	2.33 ± 0.15	1.90 ± 0.13	1.15 ± 0.170
WWD-1[a]	12	28.6	*0.293*	151 ± 5	10.8 ± 0.4	3.39	64 ± 2	21.5 ± 1.3	1.99 ± 0.14	2.28 ± 0.15	1.53 ± 0.18
COS-1[a]	12	35.2	*0.316*	181 ± 3	10.9 ± 0.3	4.38	48 ± 2	20.7 ± 1.3	1.91 ± 0.13	2.37 ± 0.14	1.61 ± 0.17
COS-2[a]	12	35.1	*0.308*	313 ± 4	18.4 ± 0.4	4.19	92 ± 3	38.4 ± 2.0	2.09 ± 0.12	2.06 ± 0.12	1.30 ± 0.16
COS-3[a]	11	34.9	*0.323*	417 ± 9	25.8 ± 0.7	4.38	133 ± 5	58.4 ± 3.1	2.27 ± 0.14	1.81 ± 0.13	1.05 ± 0.16
COS-4[a]	10	35.2	*0.306*	377 ± 7	21.9 ± 0.5	4.52	107 ± 4	48.3 ± 2.5	2.20 ± 0.12	1.91 ± 0.11	1.15 ± 0.15
COS-5[a]	10	35.2	*0.297*	455 ± 5	25.7 ± 0.6	5.14	126 ± 4	64.9 ± 3.2	2.53 ± 0.14	1.62 ± 0.12	0.86 ± 0.15
COS-29[b]	10	20.11	0.180	174 ± 5	23.0 ± 0.6	5.87	107 ± 3	62.9 ± 3.2	2.74 ± 0.16	1.51 ± 0.12	0.76 ± 0.16
COS-6[a]	9	35.1	*0.312*	459 ± 5	27.3 ± 0.6	4.73	145 ± 5	68.4 ± 3.5	2.51 ± 0.14	1.61 ± 0.12	0.86 ± 0.15
COS-25[b]	9	20.407	0.202	280 ± 2	26.0 ± 0.5	2.5	323 ± 6	80.2 ± 3.6	3.08 ± 0.15	1.26 ± 0.10	0.51 ± 0.14
COS-30[b]	9	20.076	0.180	305 ± 6	25.6 ± 0.7	3.82	179 ± 5	68.2 ± 3.4	2.66 ± 0.15	1.53 ± 0.12	0.77 ± 0.15
COS-31[b]	9	20.333	0.184	296 ± 5	25.0 ± 0.7	2.91	231 ± 10	67.2 ± 3.9	2.68 ± 0.17	1.52 ± 0.13	0.76 ± 0.17
COS-26[b]	9	20.446	0.183	310 ± 3	26.0 ± 0.6	2.7	300 ± 5	81.1 ± 3.5	3.12 ± 0.15	1.24 ± 0.10	0.49 ± 0.14
COS-27[b]	9	20.083	0.194	251 ± 2	22.7 ± 0.5	2.7	251 ± 5	67.8 ± 3.1	2.98 ± 0.15	1.36 ± 0.10	0.61 ± 0.14

[a] Measured at LLNL.
[b] Measured at CEREGE.
[c] Italic – Be spike concentration = 974 ppm; Simple – Be spike concentration = 1400 ppm. Uncertainties in concentrations include spike uncertainty added in quadrature.
[d] Corrected for AMS and procedural blanks.

Matuyama, suggesting that the cosmogenic ages in the *n1* interval may be slightly overestimated. We mark these ages with a red frame in Fig. 8A and discuss the source of this possible bias in Section 5.2. Below this, sample COS-4 (1.15 ± 0.15 Ma), which was taken near the *r1-n2* transition, fits well with the age range of the Jaramillo and the Cobb Mtn. subchrons. Sample COS-3 (1.05 ± 0.16 Ma) is located within *r2*, suggesting that it might be slightly underestimated. Similarly, COS-1 and WWD-1 also yield underestimated ages because they were collected in an area within or below Olduvai (cyan arrow in Fig. 5A). We discuss in detail the source of the bias in the corrected cosmogenic ages in Section 5.2.

The simple cosmogenic ages define maximum age constraints of the deposits, which provide independent critical age constraints to the magnetostratigraphic model. The simple age of sample COS-3, located in interval *r2* correspond to the Olduvai. Thus, the age of *r2* must be younger than the Olduvai. In addition, samples COS-1 and WWD-1 are located below the transition *r2-n3*, but their simple cosmogenic ages are significantly younger than the Matuyama-Gauss transition. This indicates that *n3* must be younger than the Gauss chron and that *n2* and *n3* are subchrons within the Matuyama. Given the slow sedimentation rate in the cave, it seems more likely that *n3* is Olduvai (~140 ky), rather than the short-term Feni (~21 ky). We note that the simple age of the lowermost sample (COS-0) is younger than the overlying samples WWD-1, COS-1, and COS-2, and therefore we do not use it as an age constraint.

After establishing the correlation of *n2* as the Jaramillo or the Cobb Mtn. and *n3* as the Olduvai, we test the magnetostratigraphic age model based on the inferred depositional rate in *r2,* bracketed by *n2* and *n3*. The depositional rate in *r2* is 1–1.3 mm/ky. This seems to be a reasonable rate considering the conditions in the cave. Using this rate, the Jaramillo (80 ky) interval would be 8–10 cm thick and shorter subchrons, like the Cobb Mtn. (35 ky) and Feni (21 ky) would be only 3–5 and 2–3 cm thick, respectively. The inferred sedimentation rate in *r2* is in agreement with the thickness of *n2* (~10 cm) that represents a short subchron (e.g. Jaramillo). However, the thickness of *r1* is inconsistent with the length of the inferred period of accumulation. As discussed above, this inconsistency suggests an erosional event or depositional hiatus associated with *r1.* In addition, the thick (>2 m) section associated with *n1* interval in Exc. 1-S would require a far more rapid rate of accumulation than the rate calculated for *r2*, as this interval is limited to the time period from the onset of the Brunhes to the end of the ESA (ca. 500-400 kyr). The thick accumulation is partly due to Units such as St. 8 which is composed of large debris of dolomite clasts. Thus, continuous sediment accumulation at a constant rate in Wonderwerk Cave must be treated with caution as there are likely periods of relative rapid accumulation punctuated by hiatuses in sediment accumulation and erosional events.

Finally, the age model which is based solely on paleomagnetism and cosmogenic burial ages, correlates well with the archaeological and biochronological findings: St. 6-11 (*n1-r1-n2*) consists of an Acheulean industry and St. 12 (*r2-n3*) assemblage is limited to Oldowan tools and contains extinct faunal species typical of the early Pleistocene that do not occur in St. 10 or later.

The new age model of Wonderwerk is based on a minimum number of assumptions and two chronological tie-points: (i) based on archaeological evidence the top of the section is younger than the Brunhes-Matuyama boundary, and (ii) the simple cosmogenic ages in St. 12 indicate that the *r2-n3* transition in St. 12 is younger than the Matuyama-Gauss boundary. Our model requires at least one hiatus associated with *r1.* Fig. 9 displays the variations of the possible extent of this hiatus assuming that it is conceivable that the Cobb Mtn. subchron is not represented in the magneto-stratigraphy. Each of these affects the age model of the onset of *n1* differently. The possibility that *n1* includes both the Bruhnes and

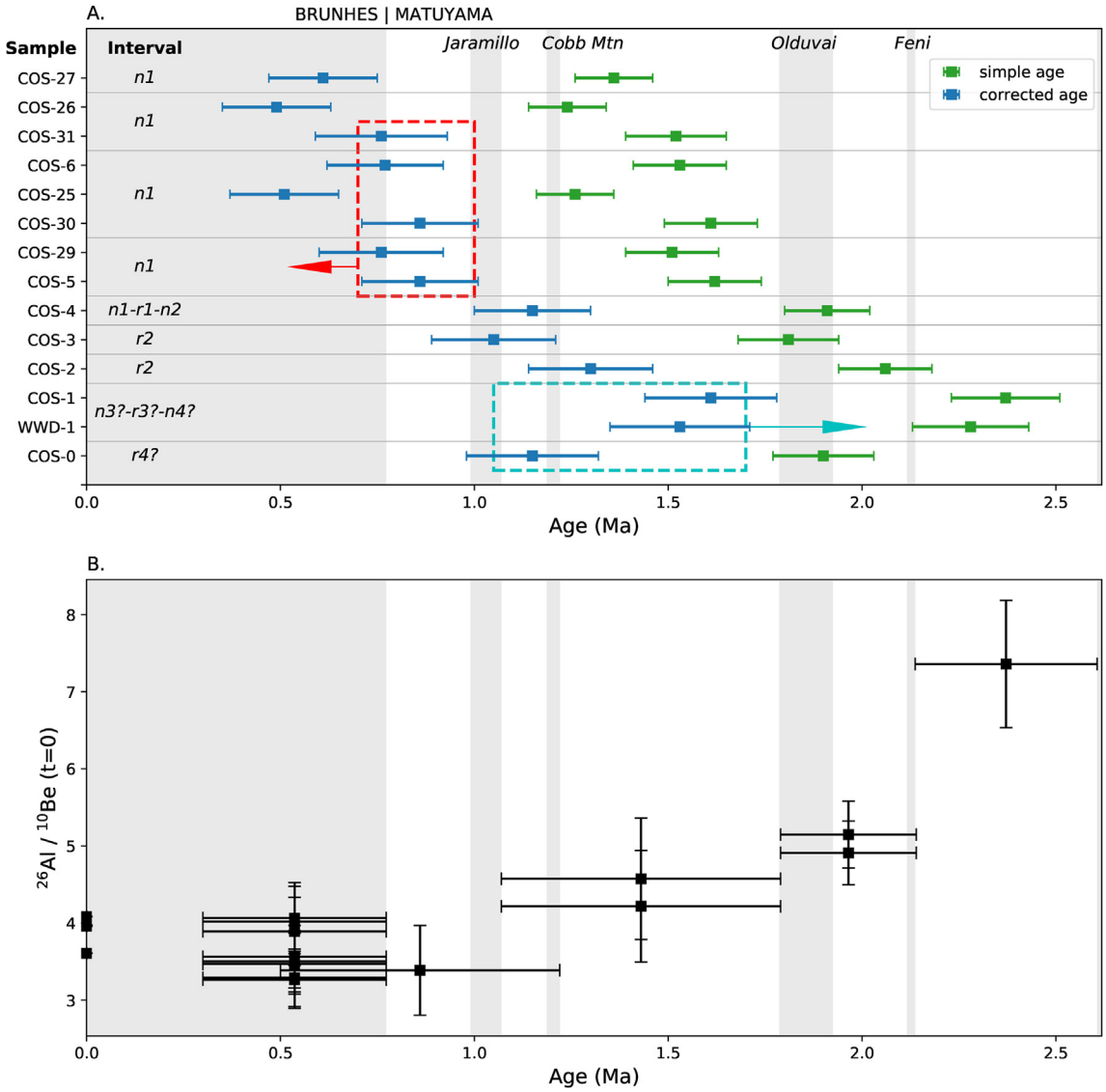

Fig. 8. Cosmogenic burial ages, polarity intervals and geomagnetic polarity time scale. A) Cosmogenic ages plotted according to stratigraphic position. Green (blue) are simple (corrected) ages respectively. Samples bracketed by horizontal lines were collected from the same horizon. Intervals labels in the left mark the magnetic polarity zones from which the samples were collected (Fig. 3A,C). Red (cyan) frames and arrows show cosmogenic isotopes that are slightly overestimated (underestimated). B) Inherited $^{26}Al/^{10}Be$ ratio of the cosmogenic samples at time of deposition, calculated using the paleomagnetic ages discussed in the text. Vertical stripes correspond to the geomagnetic polarity time scale (Channell et al., 2020) (Fig. 3C). (For interpretation of the references to colour in this figure legend, the reader is referred to the Web version of this article.)

Jaramillo would require a second hiatus as shown in Fig. 9, but this option is more complicated and is not adopted here. Yet, such an interpretation cannot be definitively rejected based on available data. As discussed below, it is important to emphasize that none of these considerations alter the age of the underlying *r2-n3*.

5.2. Temporal changes in the inherited $^{26}Al/^{10}Be$ ratio

One interesting result of the comparison between the magnetostratigraphy and the cosmogenic burial ages is that the correction of the simple cosmogenic burial ages, assuming a fixed inherited $^{26}Al/^{10}Be$ ratio for the entire section, results in a biased pattern compared to the magnetostratigraphy (Fig. 8A). The cosmogenic ages at the top of the section are slightly overestimated (dashed red frame), while the ages are underestimated at the bottom of the section (dashed cyan frame). This pattern can be explained by two different sources of uncertainty in the interpretation of the cosmogenic burial ages, each would result in an opposite trend of bias, as explained below.

First, it is possible, and perhaps likely, that the initial inherited $^{26}Al/^{10}Be$ ratio has varied with time. The stratigraphic order observed among the cosmogenic samples seems to negate the possibility of a random process governing the inherited $^{26}Al/^{10}Be$ ratio. Rather, a systematic change in the apparent burial age at the time sediment entered the cave seems possible. The underestimated ages of the lower section suggest that the inherited ratio was higher 1-2 million years ago than over the last million years. The factors that control ^{26}Al and ^{10}Be concentrations and their ratio in quartz grains are: i) their initial ^{26}Al and ^{10}Be concentrations and ratio which is the function of the erosion of bedrock from which they were derived, ii) the total time they spend in the landscape, iii) the fraction of time spent buried while passing through the landscape, and iv) the thickness of the sand sheet. These factors are discussed extensively in Vainer et al. (2018a); Vainer et al. (2018b).

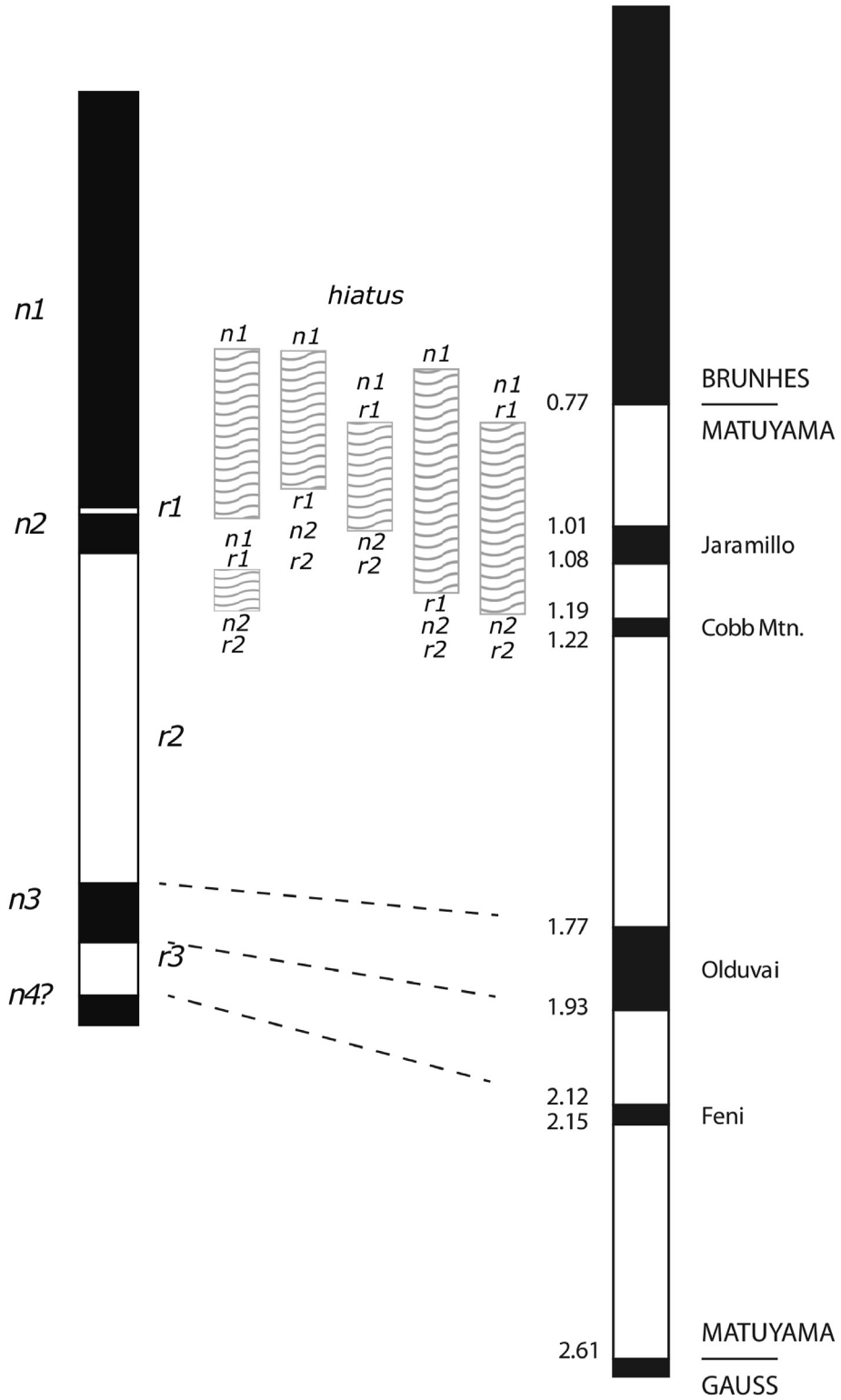

Fig. 9. Stratigraphic position of the hiatus associated with r1. See text for details.

To quantify the change in the inherited $^{26}Al/^{10}Be$ ages with time, we used the magnetostratigraphic age constraints on the cosmogenic samples to back-calculate the pre-burial $^{26}Al/^{10}Be$ ratios (Fig. 8B). Indeed, we find that generally, the inherited ratios decrease as sediments become younger. The ratio in the stratigraphically oldest cosmogenic sample (COS-0) is indistinguishable from the surface production ratio (~6.8 (Balco et al., 2008; Nishiizumi et al., 2007)). It then decreases until ~1.0 Ma and remains relatively constant over the last 1.0 Ma. Therefore, applying a uniform correction (based on the modern ratio) causes an underestimation of the corrected burial ages at the bottom of the section. This change in $^{26}Al/^{10}Be$ ratio may also be the result of dissimilar transport and depositional

conditions and processes during the deposition of the lower and older samples.

Secondly, the cosmogenic burial clock starts ticking the moment sand enters the cave. However, there is a time gap between this moment and the time that the sand actually settles and becomes part of the sequence and acquires its paleomagnetic signal. This time gap is difficult to quantify. Nevertheless, this source of uncertainty is most likely constant for all samples and will always result in the overestimation of the burial ages. This mechanism can explain the slight overestimation of the upper samples (red arrow in Fig. 8A). The magnitude of the overestimation suggests that the grains migrate from the entrance of the cave to the area of Exc. 1 (~30 m today) over a period of ~100 ky. We did not apply a correction to the burial ages that stems from this source of uncertainty.

5.3. The age of the Acheulean

One of the goals of the revised paleomagnetic and cosmogenic dating at Wonderwerk was to clarify the chronology of the Acheulean, including the age of early evidence for the use of fire (St. 10) (Berna et al., 2012), the appearance of systematic handaxe manufacture (St. 10), and the shift in the refinement of handaxes (St. 8). Previous publications (Berna et al., 2012; Chazan et al., 2008, 2012; Matmon et al., 2012) identified the entirety of St. 10 with the Jaramillo subchron and left open the possibility of an overlying reversal or depositional hiatus. Pickering (2015) dated buried speleothems within St. 10, derived from the area associated with *n1,* and provided maximum ages of 0.734 ± 0.069 Ma and 0.839 ± 0.026 Ma. These maximum ages are in agreement with the magnetostratigraphy presented here. The new chronostratigraphic data point to an apparent hiatus within St. 10, posing a difficulty in precisely defining the absolute chronology of technological developments, including the use of fire identified in St. 10 (which remains in the 1.0 Ma age range) within the Acheulean of Wonderwerk. However, the new data clearly indicate that the initial appearance of handaxes at the base of St. 11, corresponding to *r2*, is significantly older than 1.07 Ma or 1.22 Ma (the age of the top of *r2*). These results are consistent with ages for early Acheulean contexts in the Vaal gravels, dated to as old as ~1.7 Ma, based on cosmogenic burial dating reported by Gibbon et al. (2009) and Kuman and Gibbon (2018).

5.4. The age of the Oldowan

In previous publications of the paleomagnetic sequence at Wonderwerk Cave, the Oldowan was attributed to the Olduvai subchron due to the associated normal signal underlying a lengthy reverse deposit and the associated cosmogenic ages. However, as noted by Pickering (2015) it was nevertheless possible that the overlying reversal event was the interval underlying the Brunhes, so that the Oldowan deposits could date to the Jaramillo. Here, we provide strong evidence for firmly associating the Oldowan in St. 12 with the Olduvai subchron. It should be noted that the top of *n3*, shown to be the Olduvai subchron, lies within the top of lithostratigraphic Unit 9 such that the Oldowan appears to straddle the boundary between the Olduvai subchron and the overlying reversal and can therefore be placed with confidence to ca. 1.8 Ma. These results cannot be reconciled with the late age for the Oldowan and onset of the Acheulean as proposed in Herries et al. (2009); Herries and Shaw (2011) based on research at sites in the Cradle of Humankind which rests heavily on unpublished ESR ages, with no published information on uptake models or other methodological detail (Herries et al., 2009).

The age of the Oldowan, along with the timing of the initial appearance of bifaces as established in this paper for Wonderwerk Cave, confirm the temporal alignment of developments in Earlier Stone Age lithic technology in East and Southern Africa. The only exception to this pattern is the initial appearance of lithic technology, which is significantly earlier in East Africa than in southern Africa (Braun et al., 2019; Harmand et al., 2015). Acheulean lithic production in Southern Africa can now be confirmed to develop near the base of the newly defined Natronian Land Mammal Age (Van Couvering and Delson, 2020).

Wonderwerk Cave is one of a small number of sites in South Africa with an Oldowan lithic assemblage. The Wonderwerk Cave Oldowan lithic assemblage is unusual as it lacks a large tool component and is dominated by very small tools. The emphasis on small tools is also characteristic of Sterkfontein (Member 5) and Swartkrans (Member 1), although at these sites large tools are also present and the large number of small flakes is at least partially interpreted as the result of winnowing and the fracture properties of the quartzite that serves as raw material (Kuman and Field, 2009). The dominant raw material in the Wonderwerk Oldowan is chert which does not have the tendency to shatter as quartzite. It is important to emphasize that the Wonderwerk Oldowan assemblage, as with the Sterkfontein (Kuman and Field, 2009) and Swartkrans (Kuman et al., 2018) assemblages, includes both small flakes and the cores for the production of these flakes. Micromorphological analysis indicates only low energy water transport that would not be adequate to produce a winnowed assemblage (Goldberg et al., 2015). Both lithics and fauna show no signs of abrasion resulting from water transport and the faunal elements include both large and small-sized species (micro-mammals) and different sized skeletal elements showing no selection that can be attributed to water winnowing.

The results from Wonderwerk Cave reported here, along with consistent data from Sterkfontein and Swartkrans, are critical for setting the timescale for the early stages of the ESA in Southern Africa but also for determining the correlation of these industries with hominin species, and the timing of the last appearance of *Paranthropus*. The dating of the Oldowan of Member 5 at Sterkfontein to ca. 2–1.7 Ma (Gibbon et al., 2009; Kuman and Clarke, 2000) is now strongly supported by the combined magnetostratigraphy and cosmogenic burial age dating of Wonderwerk Cave.

6. Summary and conclusions

This article reports the results of paleomagnetic and cosmogenic burial dating at Excavation 1, Wonderwerk Cave, South Africa, updating previously reported results (Matmon et al., 2012) with analysis of additional seven cosmogenic ages and 282 paleomagnetic samples. From a total of 323 paleomagnetic samples in Exc. 1-N and Exc. 1-S, 178 samples pass our selection criteria with MAD <15, DANG <30 and angular deviation from GAD field <45°. These data enabled the construction of a revised age model that provides an improved chronological framework for one of the longest sedimentary sequences of the Earlier Stone Age in Southern Africa.

The stratigraphic sequence, spanning the past ~2.0 Ma includes at least one hiatus in the Acheulean St. 10, posing difficulty in precise interpretation of the magnetostratigraphy. Nevertheless, we identify two paleomagnetic chronological markers that anchor the stratigraphy of Exc. 1: (i) a reversal at the base of St. 10 of the Acheulean sequence, which underlies either the Jaramillo (1.07 Ma) or the Cobb Mtn. subchrons (1.22 Ma), and (ii) a normal interval in the upper part of the Oldowan St. 12, marking the Olduvai subchron (1.77–1.93 Ma). The sedimentation rate between these anchors is 1–1.3 mm/ky.

The cosmogenic burial ages are corrected for the inherited

$^{26}Al/^{10}Be$ ratio of the particles entering the cave using the mean of the measured ratios in four sand samples collected outside the cave, which represent the $^{26}Al/^{10}Be$ ratios of today's sediments. A simple correction of the cosmogenic ages using this mean ratio yields underestimated ages for samples older than ~1.0 Ma. This underestimation suggests a different aeolian regime in the Kalahari during the Early to Middle Pleistocene, in which sand may have been transported faster and buried shallower, or for less time, during transport. A change in the environmental conditions after the deposition of St. 12 is also supported by the occurrence of hematite only in St. 12. The slightly overestimated burial ages at the top of the section, suggest that the particles migrated inside the cave over a period of about 100 ky before finally settling. The data suggests that the application of a homogeneous inheritance dose model for a lengthy sedimentary sequence, should be applied with some caution.

The Oldowan industry in St. 12 (Unit 9) is correlated with the Olduvai subchron (1.77–1.93), while the onset of the Acheulean in St. 11 is older than ca. 1.07 Ma (possibly older than ca. 1.22 Ma). These results offer strong support for an early age for the Oldowan of Southern Africa and a degree of synchronicity in the development of archaeological industries between Southern Africa and East Africa. The Oldowan industries of South Africa are contemporaneous with fossils of *Paranthropus*, early *Homo*, and *Australopithecus sediba* and so as in East Africa, are associated with a period of phylogenetic diversity in the hominin lineage.

Author contributions

M.C and L.K.H initiated and designed the project, directed the archaeological campaigns and led field work; R.S carried out the paleomagnetic analyses, made the figures and led the manuscript writing; A.M carried out the cosmogenic isotopes analyses; Y.E. assisted with the paleomagnetic analyses; All authors contributed equally to final data analyses and to manuscript writing.

Declaration of competing interest

The authors declare that they have no known competing financial interests or personal relationships that could have appeared to influence the work reported in this paper.

Acknowledgments

Research at Wonderwerk Cave is carried out under permit from the South African Heritage Resources Agency. We are grateful for support from David Morris, head of the Department of Archaeology, McGregor Museum. Funding for this research is provided by grants from the Canadian Social Sciences and Humanities Research Council and the Paleontological Scientific Trust. We thank two anonymous reviewers for their insightful comments on this manuscript and Darryl Granger for reviewing two versions of this work and for suggestions that significantly improved the manuscript.

Appendix A. Supplementary data

Supplementary data to this article can be found online at https://doi.org/10.1016/j.quascirev.2021.106907.

References

Albarede, F., Balter, V., Braga, J., Blichert-Toft, J., Telouk, P., Thackeray, F., 2006. U-Pb dating of enamel from the Swartkrans Cave hominid site (South Africa) by MC-ICP-MS. Geochem. Cosmochim. Acta 70. A7-A7.

Argento, D.C., Reedy, R.C., Stone, J.O., 2013. Modeling the earth's cosmic radiation. Nucl. Instrum. Methods Phys. Res. Sect. B Beam Interact. Mater. Atoms 294, 464–469.

Balco, G., Stone, J.O., Lifton, N.A., Dunai, T.J., 2008. A complete and easily accessible means of calculating surface exposure ages or erosion rates from Be-10 and Al-26 measurements. Quat. Geochronol. 3, 174–195.

Beaumont, P.B., Vogel, J.C., 2006. On a timescale for the past million years of human history in central South Africa. South Afr. J. Sci. 102, 217–228.

Berna, F., Goldberg, P., Horwitz, L.K., Brink, J., Holt, S., Bamford, M., Chazan, M., 2012. Microstratigraphic evidence of in situ fire in the Acheulean strata of Wonderwerk cave, northern Cape province, South Africa. Proc. Natl. Acad. Sci. U.S.A. 109, E1215–E1220.

Bierman, P.R., Caffee, M., 2001. Slow rates of rock surface erosion and sediment production across the Namib Desert and escarpment, southern Africa. Am. J. Sci. 301, 326–358.

Braun, D.R., Aldeias, V., Archer, W., Arrowsmith, J.R., Baraki, N., Campisano, C.J., Deino, A.L., DiMaggio, E.N., Dupont-Nivet, G., Engda, B., Feary, D.A., Garello, D.I., Kerfelew, Z., McPherron, S.P., Patterson, D.B., Reeves, J.S., Thompson, J.C., Reed, K.E., 2019. Earliest known Oldowan artifacts at > 2.58 Ma from Ledi-Geraru, Ethiopia, highlight early technological diversity. Proc. Natl. Acad. Sci. U.S.A. 116, 11712–11717.

Brink, J., Holt, S., Horwitz, L.K., 2016. The Oldowan and early Acheulean Mammalian fauna of Wonderwerk cave (Northern Cape Province, South Africa). Afr. Archaeol. Rev. 33, 223–250.

Channell, J.E.T., Singer, B.S., Jicha, B.R., 2020. Timing of Quaternary geomagnetic reversals and excursions in volcanic and sedimentary archives. Quat. Sci. Rev. 228, 106114.

Chazan, M., 2015. Technological trends in the Acheulean of Wonderwerk Cave, South Africa. Afr. Archaeol. Rev. 32, 701–728.

Chazan, M., Avery, D.M., Bamford, M.K., Berna, F., Brink, J., Fernandez-Jalvo, Y., Goldberg, P., Holt, S., Matmon, A., Porat, N., Ron, H., Rossouw, L., Scott, L., Horwitz, L.K., 2012. The Oldowan horizon in Wonderwerk Cave (South Africa): archaeological, geological, paleontological and paleoclimatic evidence. J. Hum. Evol. 63, 859–866.

Chazan, M., Berna, F., Brink, J., Ecker, M., Holt, S., Porat, N., Lee-Thorp, J.A., Horwitz, L.K., 2020. Archeology, environment, and chronology of the early Middle stone age component of Wonderwerk cave. J. Paleolithic Archaeol. 3, 302–335.

Chazan, M., Ron, H., Matmon, A., Porat, N., Goldberg, P., Yates, R., Avery, M., Sumner, A., Horwitz, L.K., 2008. Radiometric dating of the earlier Stone Age sequence in excavation I at Wonderwerk Cave, South Africa: preliminary results. J. Hum. Evol. 55, 1–11.

Chmeleff, J., von Blanckenburg, F., Kossert, K., Jakob, D., 2010. Determination of the Be-10 half-life by multicollector ICP-MS and liquid scintillation counting. Nucl. Instrum. Methods B 268, 192–199.

Dirks, P.H.G.M., Berger, L.R., 2013. Hominin-bearing caves and landscape dynamics in the Cradle of Humankind, South Africa. J. Afr. Earth Sci. 78, 109–131.

Dirks, P.H.G.M., Roberts, E.M., Hilbert-Wolf, H., Kramers, J.D., Hawks, J., Dosseto, A., Duval, M., Elliott, M., Evans, M., Grun, R., Hellstrom, J., Herries, A.I.R., Joannes-Boyau, R., Makhubela, T.V., Placzek, C.J., Robbins, J., Spandler, C., Wiersma, J., Woodhead, J., Berger, L.R., 2017. The age of *Homo naledi* and associated sediments in the Rising Star Cave, South Africa. Elife 6.

Ecker, M., Brink, J., Chazan, M., Horwitz, L.K., Lee-Thorp, J.A., 2017. Radiocarbon dates constrain the timing of environmental and cultural shifts in the Holocene strata of Wonderwerk Cave, South Africa. Radiocarbon 59, 1067–1086.

Fourvel, J.B., Brink, J., O'Regan, H., Beaudet, A., Pavia, M., 2016. Some preliminary interpretations of the oldest faunal assemblage from Kromdraai. In: Braga, J., Thackeray, J.F. (Eds.), Kromdraai: A Birthplace of Paranthropus in the Cradle of Humankind. AFRICAN SUN MeDIA, pp. 71–106.

Gentry, A., 2010. Bovidae. In: Werdelin, L., Sanders, J. (Eds.), Cenozoic Mammals of Africa. Univ of California Press, pp. 747–803.

Gibbon, R.J., Granger, D.E., Kuman, K., Partridge, T.C., 2009. Early Acheulean technology in the Rietputs Formation, South Africa, dated with cosmogenic nuclides. J. Hum. Evol. 56, 152–160.

Gibbon, R.J., Pickering, T.R., Sutton, M.B., Heaton, J.L., Kuman, K., Clarke, R.J., Brain, C.K., Granger, D.E., 2014. Cosmogenic nuclide burial dating of hominin-bearing Pleistocene cave deposits at Swartkrans, South Africa. Quat. Geochronol. 24, 10–15.

Goldberg, P., Berna, F., Chazan, M., 2015. Deposition and diagenesis in the Earlier Stone Age of Wonderwerk Cave, excavation 1, South Africa. Afr. Archaeol. Rev. 32, 613–643.

Granger, D.E., 2006. A review of burial dating methods using 26Al and 10Be. Spec. Pap. Geol. Soc. Am. 415.

Granger, D.E., Gibbon, R.J., Kuman, K., Clarke, R.J., Bruxelles, L., Caffee, M.W., 2015. New cosmogenic burial ages for Sterkfontein Member 2 *Australopithecus* and Member 5 Oldowan. Nature 522, 85–U200.

Granger, D.E., Kirchner, J.W., Finkel, R.C., 1997. Quaternary downcutting rate of the New River, Virginia, measured from differential decay of cosmogenic Al-26 and Be-10 in cave-deposited alluvium. Geology 25, 107–110.

Granger, D.E., Muzikar, P.F., 2001. Dating sediment burial with in situ-produced cosmogenic nuclides: theory, techniques, and limitations. Earth Planet Sci. Lett. 188, 269–281.

Grun, R., Brink, J.S., Spooner, N.A., Taylor, L., Stringer, C.B., Franciscus, R.G., Murray, A.S., 1996. Direct dating of Florisbad hominid. Nature 382, 500–501.

Harmand, S., Lewis, J.E., Feibel, C.S., Lepre, C.J., Prat, S., Lenoble, A., Boes, X.,

Quinn, R.L., Brenet, M., Arroyo, A., Taylor, N., Clement, S., Daver, G., Brugal, J.P., Leakey, L., Mortlock, R.A., Wright, J.D., Lokorodi, S., Kirwa, C., Kent, D.V., Roche, H., 2015. 3.3-million-year-old stone tools from Lomekwi 3, west Turkana, Kenya. Nature 521, 310–315.
Herries, A.I.R., Curnoe, D., Adams, J.W., 2009. A multi-disciplinary seriation of early *Homo* and *Paranthropus* bearing palaeocaves in southern Africa. Quat. Int. 202, 14–28.
Herries, A.I.R., Shaw, J., 2011. Palaeomagnetic analysis of the Sterkfontein palaeocave deposits: implications for the age of the hominin fossils and stone tool industries. J. Hum. Evol. 60, 523–539.
Hidy, A.J., Gosse, J.C., Blum, M.D., Gibling, M.R., 2014. Glacial-interglacial variation in denudation rates from interior Texas, USA, established with cosmogenic nuclides. Earth Planet Sci. Lett. 390, 209–221.
Horwitz, L.K., Chazan, M., 2015. Past and present at Wonderwerk Cave (Northern Cape province, South Africa). Afr. Archaeol. Rev. 32, 595–612.
Kirschvink, J.L., 1980. The least-squares line and plane and the analysis of paleomagnetic data. Geophys. J. Roy. Astron. Soc. 62, 699–718.
Kohl, C.P., Nishiizumi, K., 1992. Chemical isolation of quartz for measurement of Insitu-produced cosmogenic nuclides. Geochem. Cosmochim. Acta 56, 3583–3587.
Korschinek, G., Bergmaier, A., Faestermann, T., Gerstmann, U.C., Knie, K., Rugel, G., Wallner, A., Dillmann, I., Dollinger, G., von Gostomski, C.L., Kossert, K., Maiti, M., Poutivtsev, M., Remmert, A., 2010. A new value for the half-life of Be-10 by Heavy-Ion Elastic Recoil Detection and liquid scintillation counting. Nucl. Instrum. Methods B 268, 187–191.
Kuman, K., Clarke, R.J., 2000. Stratigraphy, artefact industries and hominid associations for Sterkfontein, Member 5 (vol 38, pg 827, 2000). J. Hum. Evol. 39, 267-267.
Kuman, K., Field, A.S., 2009. The Oldowan industry from Sterkfontein Caves, South Africa. In: Schick, K., Toth, N. (Eds.), The Cutting Edge: New Approaches to the Archaeology of Human Origins.
Kuman, K., Gibbon, R.J., 2018. The Rietputs 15 site and early Acheulean in South Africa. Quat. Int. 480, 4–15.
Kuman, K., Sutton, M.B., Pickering, T.R., Heaton, J.L., 2018. The Oldowan industry from Swartkrans Cave, South Africa, and its relevance for the African Oldowan. J. Hum. Evol. 123, 52–69.
Lifton, N., Sato, T., Dunai, T.J., 2014. Scaling *in situ* cosmogenic nuclide production rates using analytical approximations to atmospheric cosmic-ray fluxes. Earth Planet Sci. Lett. 386, 149–160.
Liu, Q., Roberts, A.P., Larrasoana, J.C., Banerjee, S.K., Guyodo, Y., Tauxe, L., Oldfield, F., 2012. Environmental magnetism: principles and applications. Rev. Geophys. 50.
Matmon, A., Fink, D., Davis, M., Niedermann, S., Rood, D., Frumkin, A., 2014. Unraveling rift margin evolution and escarpment development ages along the Dead Sea fault using cosmogenic burial ages. Quat. Res. 82, 281–295.
Matmon, A., Hidy, A.J., Vainer, S., Crouvi, O., Fink, D., Erel, Y., Horwitz, L.K., Chazan, M., Team, A., 2015. New chronology for the southern Kalahari Group sediments with implications for sediment-cycle dynamics and early hominin occupation. Quat. Res. 84, 118–132.
Matmon, A., Ron, H., Chazan, M., Porat, N., Horwitz, L.K., 2012. Reconstructing the history of sediment deposition in caves: a case study from Wonderwerk Cave, South Africa. Geol. Soc. Am. Bull. 124, 611–625.
Mcfadden, P.L., Brock, A., Partridge, T.C., 1979. Paleomagnetism and the age of the Makapansgat hominid site. Earth Planet Sci. Lett. 44, 373–382.
Nishiizumi, K., 2004. Preparation of Al-26 AMS standards. Nucl. Instrum. Methods B 223, 388–392.
Nishiizumi, K., Imamura, M., Caffee, M.W., Southon, J.R., Finkel, R.C., McAninch, J., 2007. Absolute calibration of Be-10 AMS standards. Nucl. Instrum. Methods B 258, 403–413.
Partridge, T.C., Maud, R.R., 2000. Macro-scale geomorphic evolution of southern Africa. Oxf. Monogr. Geol. Geophys. 40, 3–18.
Pickering, R., 2015. U-Pb dating small buried stalagmites from Wonderwerk Cave, South Africa: a new chronometer for Earlier Stone Age cave deposits. Afr. Archaeol. Rev. 32, 645–668.
Pickering, R., Kramers, J.D., Hancox, P.J., de Ruiter, D.J., Woodhead, J.D., 2011. Contemporary flowstone development links early hominin bearing cave deposits in South Africa. Earth Planet Sci. Lett. 306, 23–32.
Pickering, R., Kramers, J.D., Partridge, T., Kodolanyi, J., Pettke, T., 2010. U-Pb dating of calcite-aragonite layers in speleothems from hominin sites in South Africa by MC-ICP-MS. Quat. Geochronol. 5, 544–558.
Porat, N., Chazan, M., Grun, R., Aubert, M., Eisenmann, V., Horwitz, L.K., 2010. New radiometric ages for the Fauresmith industry from Kathu Pan, southern Africa: implications for the Earlier to Middle Stone Age transition. J. Archaeol. Sci. 37, 269–283.
Rasmussen, D.T., Gutiérrez, M., 2010. In: Werdelin, L., Sanders, J. (Eds.), Cenozoic Mammals of Africa. Univ of California Press, pp. 123–145.
Ruther, H., Chazan, M., Schroeder, R., Neeser, R., Held, C., Walker, S.J., Matmon, A., Horwitz, L.K., 2009. Laser scanning for conservation and research of African cultural heritage sites: the case study of Wonderwerk Cave, South Africa. J. Archaeol. Sci. 36, 1847–1856.
Tauxe, L., Banerjee, S.K., Butler, R.F., Van der Voo, R., 2018. Essentials of Paleomagnetism, 5th Web ed.
Tauxe, L., Shaar, R., Jonestrask, L., Swanson-Hysell, N.L., Minnett, R., Koppers, A.A.P., Constable, C.G., Jarboe, N., Gaastra, K., Fairchild, L., 2016. PmagPy: software package for paleomagnetic data analysis and a bridge to the magnetics information Consortium (MagIC) database. G-cubed 17, 2450–2463.
Tauxe, L., Staudigel, H., 2004. Strength of the geomagnetic field in the Cretaceous normal Superchron: new data from submarine basaltic glass of the Troodos Ophiolite. G-cubed 5.
Thackeray, J.F., Kirschvink, J.L., Raub, T.D., 2002. Palaeomagnetic analyses of calcified deposits from the Plio-Pleistocene hominid site of Kromdraai, South Africa. South Afr. J. Sci. 98, 537–540.
Thebault, E., Finlay, C.C., Alken, P., Beggan, C.D., Canet, E., Chulliat, A., Langlais, B., Lesur, V., Lowes, F.J., Manoj, C., Rother, M., Schachtschneider, R., 2015. Evaluation of candidate geomagnetic field models for IGRF-12. Earth Planets Space 67.
Vainer, S., Ben Dor, Y., Matmon, A., 2018a. Coupling cosmogenic nuclides and luminescence dating into a unified accumulation model of aeolian landforms age and dynamics: the case study of the Kalahari Erg. Quat. Geochronol. 48, 133–144.
Vainer, S., Erel, Y., Matmon, A., 2018b. Provenance and depositional environments of Quaternary sediments in the southern Kalahari Basin. Chem. Geol. 476, 352–369.
Van Couvering, J., Delson, E., 2020. African Land Mammal Ages: definition and inclusion of primate range data. Am. J. Phys. Anthropol. 171, 292–293.
Woodborne, S., 2016. Dating the southern African landscape. In: Knight, J., Grab, S.W. (Eds.), Quaternary Environmental Change in Southern Africa. Cambridge University Press, pp. 99–120.
Zijderveld, J.D.A., 1967. AC demagnetization of rocks: analysis of results. In: Collinson, D.W., Creer, K.M., Runcorn, S.M. (Eds.), Methods in Palaeomagnetism. Elsevier, Amsterdam.